N82 23454

Studies of the Nuclear Equation of State Using Numerical Calculations of Nuclear Drop Collisions

C. T. Alonso, J. M. LeBlanc, and J. R. Wilson
Lawrence Livermore National Laboratory, P. O. Box 808, L-18, Livermore, CA. 94550

Abstract

A numerical calculation for the full thermal dynamics of colliding nuclei has been developed. Preliminary results are reported for the thermal fluid dynamics in such processes as Coulomb scattering, fusion, fusion-fission, bulk oscillations, compression with heating, and collisions of heated nuclei.

I. Introduction

The preceding paper by Ray Nix summarized high-energy nuclear collision calculations using relativistic fluid dynamics. In this paper we shall discuss lower-energy nuclear collisions, and we shall change the emphasis from predicting outgoing multi-particle distributions to attempting to calculate the interior thermal properties of the nuclear fluid during and after a collision process. We present this study as an example of a methodology for treating the dynamics of any hot compressible fluid drop with known material properties. In our particular case we have arrived at the material properties of our exotic nuclear fluid by solving a meson field equation integrally with the thermal dynamics. For more common materials the thermal fluid dynamic methods presented here can be used in a more straightforward manner with an analytical equation of state.

The original motivation for this study came, not from nuclear physics or from fluid dynamics, but from a critical problem in astrophysics: as increasingly more accurate modelling is being included in calculations of stellar collapse, it is becoming more difficult to get those calculations to result in a supernova explosion (1). The calculations end, not with a bang, but with a whimper. Supernova explosions, while not a common sight, are definately known to occur, of course, and the astrophysicists amongst us would like to be able to predict when they occur.

A major remaining uncertainty in stellar collapse calculations is the equation of state of nuclear matter (NEOS). The equation of state is a fundamental relationship between the pressure and the density and internal energy of a fluid. In order to predict supernova explosions, the current collapse calculations of J. Wilson seem to demand rather radical departures from the currently fashionable NEOS.

The material description of a star nearing the end of its collapse is given in Table I. At densities around 10^{14} gm/cm^3 the constituent nuclei are almost touching and the temperature of the nuclear material is around 8 - 10 MeV. The heat capacity of the nucleus will determine whether the nuclei can thermally disintegrate under these conditions. Thermal disintegration is important because a free nucleon gas creates extra thermal pressures that help to generate an explosion.

Heavy nuclei, in the laboratory at least, exhibit a large number of excited states, and their extrapolated heat capacity appears to be so large that the nuclear matter is too "stiff" during collapse, producing non-exploding stars. While we don't understand all the implications at this time, J. Wilson's collapse computations might be interpreted to mean that supernova explosions require a "softer" NEOS at high densities and temperatures than current nuclear theory predicts.

Until recently, laboratory heavy-ion experiments were confined to nuclear matter near zero temperatures, and extrapolations to higher densities and temperatures led to widely varying results. During the last decade, however, high-energy heavy-ion accelerators have allowed nuclear researchers to observe experimentally the collisions of heavy nuclei and their subsequent excitation and breakup. The goal from the NEOS point of view is to obtain some information about the heating and compression of the composite nuclear fluid before it disintegrates. In heavy ion collisions excitation temperatures as high as 80 MeV are not uncommon (as deduced from the Maxwellian distribution of the emitted fragments; see Figure 1) (2). At low excitation energies the temperature dependence is that of a Fermi gas and at high excitations the temperature follows a classical Boltzmann gas law. High compressions have not yet been definitively observed, though there is intense interest in creating high compression because of a theoretically-predicted phase transition at about twice normal density. At this density the nuclear matter might exhibit a pion condensation, a state which contains many bound pions. Even higher compression might lead to a "density isomer", a stable state of very high density (3).

Thus it is extremely important, for the astrophysicist as well as for the nuclear physicist, that we understand the NEOS at high densities and temperatures. One way to approach this understanding is to adopt a NEOS and study its consequences for heavy ion collisions, looking for predicted phenomena that will help to pin down the exact form of the NEOS. We have begun such a study. In the next section we describe the NEOS approach taken by J. Wilson for our initial studies.

Mass	15 M_{sun}
Temperature	8-10 MeV
Density	2-5 X 10^{14} gm/cm^3
Infall	50,000 km/sec
Radius (Fe core)	10^8 cm
Time since Fe burn depletion	0.3 sec
Neutrino radiation rate (equivalent of visible luminosity of 10^{10} of the largest galaxies in the universe)	10^{47} W

Table I: Stellar collapse conditions just before bounce.

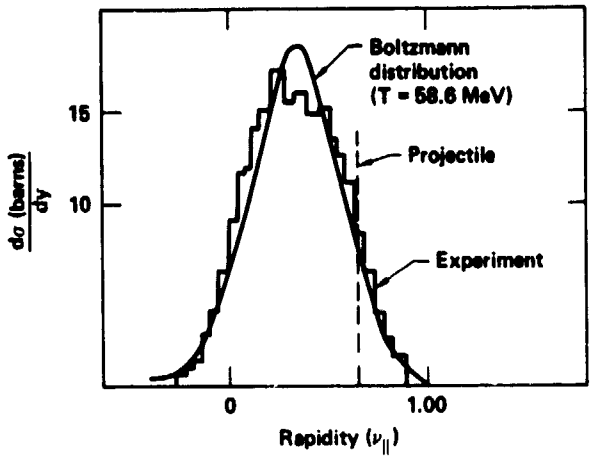

Figure 1: Maxwellian distribution of fragments from the heavy-ion collision ^{20}Ne on ^{238}U at 250 MeV/amu.

II. The Equation of State

There are at present two approaches generally used to represent the NEOS: first, the use of effective two-nucleon potentials such as the Skyrme interaction (4); and second, a direct calculation of the equilibrium energy per nucleon in terms of the underlying meson field such as the Walecka NEOS (5). All nuclear fluid dynamics (NFD) calculations up to the present have used the first approach; in this paper we report preliminary results from an effort to use the second approach in conjunction with NFD.

The Wilson nuclear equation of state used in this work was derived by solving the classical meson field equations using a Lagrangian energy density given by

$$\mathcal{L} = \frac{1}{2}\left[g^{ij}\left(\frac{\partial\phi}{\partial x^i}\frac{\partial\phi}{\partial x^j} + \frac{\partial\psi}{\partial x^i}\frac{\partial\psi}{\partial x^j}\right) + m_*^2\phi^2\right] + \rho + \epsilon + g\rho\phi + 4\pi eZ\psi \qquad (1)$$

where ϕ is a scalar field with effective mass $m_*=m_\pi(1+\rho/\rho_0)$, Ψ represents the electrostatic field, and ρ_0 and g are adjustable parameters. The density of nuclear matter is ρ, the internal energy per nucleon is ϵ, and Ze is the electric charge per nucleon. This choice of Lagrangian was motivated mostly by a desire for simplicity since our lengthy two-dimensional calculations include both dynamic and thermal effects. Also it was felt that the astrophysical calculations for which this model was intended contained greater uncertainties in other quantities than would be introduced by this simple but partially ad hoc Lagrangian.

Whereas the standard approach begins with a microscopic Lagrangian and eliminates the quantum meson fields by replacing them with classical averages, Wilson's approach begins with a combination of microscopic fields and macroscopic densities which is designed to reproduce most of the known properties of nuclear matter. In particular, by including the density-dependent effective meson m_*, he retrieves in a simple manner the saturation properties induced by the repulsive vector field in more elaborate models.

Wilson's approach is related to the Thomas-Fermi class of approximations used in nuclear and atomic theory. The use of this unusual means of arriving at the equation of state has to be justified by a comparison with more refined NEOS models and with experimental data.

Our NEOS parameters are determined by fitting the dimensionless variables g, ρ_o, and m so that they reproduce the binding energy, the measured density profiles, and the period of compressible radial oscillations ("breathing mode"), for the complete spectrum of nuclear masses. The fitted values are g=0.68, ρ_o=0.32, and m=0.73. It is a significant achievement that a model with these three constants alone can reproduce all of the above data. Figure 2 shows the resulting binding energy vs. mass curve compared with experimental values. Figure 3 compares the predicted density profiles for ^{208}Pb and ^{56}Fe with the experimentally deduced profiles. The equation of state is plotted in Figure 4. The compressibility implied by this NEOS is 200 MeV, which is close to the experimental value of 210 MeV. For comparison we also show in Figure 4 the state-of-the-art (zero-temperature) NEOS of Walecka (5) as well as the Skyrme NEOS used by Stocker et.al. in their recent studies of nuclear collisions (6). The latter implies a rather high compressibility of 295 MeV, and the Walecka NEOS is even stiffer at higher densities. The Wilson NEOS used in our studies is relatively soft, which may be more appropriate for supernova applications.

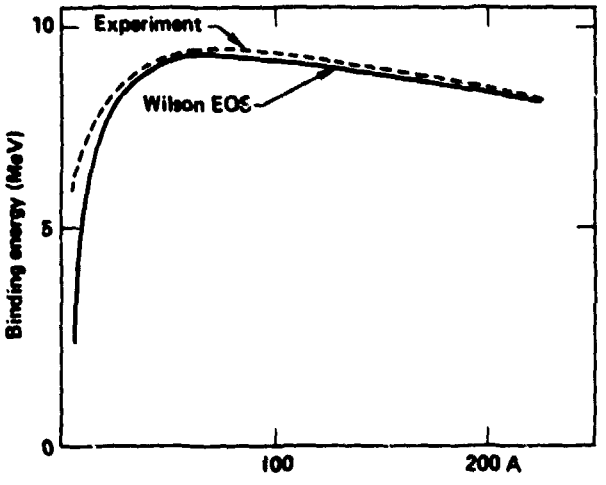

Figure 2: Comparison of experimental binding energies with Wilson's predictions for all masses A.

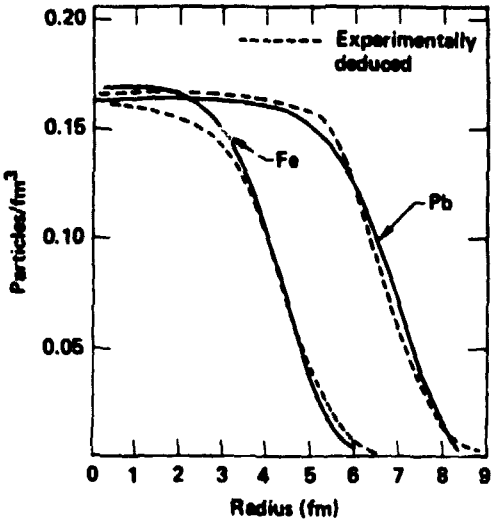

Figure 3: Density profiles for Fe and Pb predicted by the Wilson nuclear equation of state.

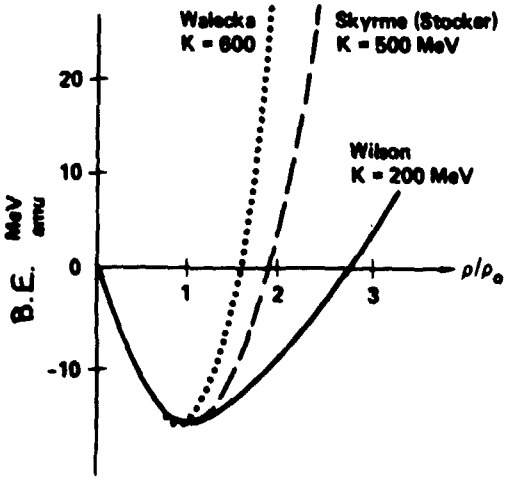

Figure 4: Comparison of current equations of state.

The work presented in this paper represents ongoing studies of dynamic heavy-ion collision processes. These studies compare our predictions using the above Wilson NEOS with experimental data and with the results of other dynamic models. Our main goals are to evaluate the consequences of this NEOS and to explore the effects of temperature, density and pressure gradients on the collision dynamics, both for cold and hot nuclear matter. These calculations are unique in that they simultaneously treat the full macroscopic thermal and dynamic fluid processes, including shock waves, while directly solving a classical scalar meson field equation for the nuclear binding. While the results shown here are for central collisions of inviscid identical nuclei, we also have the capability of treating central collisions of any two nuclei with classical viscosity.

III. Thermal Physics

Many effective interactions used in current NFD calculations include compressional but not thermal effects. The compressional part of the internal energy is usually represented by a three or four-term expansion of the internal energy as powers of the local density. In our calculations we treat both thermal and compressional contributions to the internal energy. The compressional contributions are calculated directly from the meson field Lagrangian as a function of the internal energy, as described above; the thermal contributions are calculated as described below.

Thermal effects are included in these calculations by directly computing thermal pressures, using the thermal energy of a nonrelativistic Fermi gas:

$$\epsilon_{th} = \int (P_{th} + Q) dV \tag{2}$$

Here Q is a tensor von-Neumann artificial viscosity. The pressure is obtained from a $\gamma=5/3$ law:

$$P_{th} = \frac{2}{3} \rho \epsilon_{th} \tag{3}$$

This equation is valid for all temperatures. The degeneracy energy a[illegible]ssure are given by

$$\epsilon_{deg} = \rho^{2/3} \left[z^{5/3} + (1-z)^{5/3} \right] \tag{4}$$

and

$$P_{deg} = \frac{2}{3} \rho \epsilon_{deg} \tag{5}$$

in units where $\ell = 10^{-13}$ cm, $t = 1/3 \times 10^{-23}$ sec, and m = 1 amu (the velocity of light is unity).

The temperature is not an explicit variable, so we obtain it from the internal ener[illegible] through a temperature-defining relation given by:

$$\epsilon_{total} = \epsilon_{deg} + \epsilon_{th} = \left[\epsilon_{deg}^2 + \frac{aT^2 + bT^4}{1 + cT^2} \right]^{1/2} \tag{6}$$

The constants a, b, and c were derived theoretically to give the correct expression in the limit of a cool Fermi gas ($x=kT/\epsilon_{deg}$):

$$\epsilon_{th} = 1 + \frac{3}{10} \pi^2 x^2 \tag{7}$$

the correct expression in the limit of a hot Boltzmann gas:

$$\epsilon_{th} = \frac{3}{2} x \tag{8}$$

and the exact thermal energy in the transition region where the chemical potential is equal to kT.

Thus this temperature-defining relation has been fitted to vary smoothly from low to high temperature regimes. The appropriate numerical values are a = 2.96, b = 1.5, and c = 0.66.

IV. Computational Method

To solve the full thermal dynamical problem, J. LeBlanc has employed sophisticated hybrid Eulerian-Lagrangian finite difference techniques developed over the years at the Lawrence Livermore National Laboratory. Three conservation equations are solved simultaneously in an Eulerian frame:

(1) the equation of continuity

$$\frac{d\rho}{dt} = \frac{\partial \rho}{\partial t} + \bar{u}\cdot\bar{\nabla}\rho = -\rho\,\bar{\nabla}\cdot\bar{u} \tag{9}$$

(2) energy conservation

$$\frac{d\,\rho\epsilon_{th}}{dt} = \frac{\partial \rho\epsilon_{th}}{\partial t} + \bar{u}\cdot\bar{\nabla}\rho\epsilon_{th} = -\rho\epsilon_{th}\bar{\nabla}\cdot\bar{u} - (P_{th} + Q)\bar{\nabla}\cdot\bar{u} \tag{10}$$

(3) momentum conservation

$$\frac{d\rho\bar{u}}{dt} = \frac{\partial \rho\bar{u}}{\partial t} + \bar{u}\cdot\nabla\rho\bar{u} = -\nabla(P_{tot} + Q)$$
$$-\rho\nabla\left[g\phi + \frac{g\phi^2}{\rho_0}m^2(1+\rho/\rho_0) + eZ\psi\right] \tag{11}$$

where Q is the von Neumann artificial viscosity for shocks. The fields ϕ and Ψ are solved by iterating two Poisson's equations:

(4) meson field: $\nabla^2\phi - m_*^2\phi = g\rho$ where $m_* = m(1+\rho/\rho_0)$ (12)

(5) electrostatic field: $\nabla^2\psi = 4\pi\rho Ze$ (13)

These five equations represent the full thermal dynamics of this compressible system.

In our calculations the fundamental variables are the pressures; the internal energy is calculated from $P_{th}dV$, while the zone accelerations are calculated from P_{total}, which includes the degeneracy pressure. Leaving out some technical details, we could describe this process as taking γ-law excursions off the T=0 degeneracy adiabat.

Figure 5 displays the sequential operations performed by the computer code. The Eulerian mesh typically contains around 2000 nodes (the dots shown in the graphics). The basic Lagrangian parts (the pressures and accelerations at time t) are calculated first. Next the Eulerian terms are calculated using a second-order accurate implicit scheme on two staggered time-levels. Finally the meson and electrostatic fields are calculated using an overrelaxation method. The whole calculation is extremely fast, taking on the average 60 μsec/cycle on a 7600. The time step δt is calculated according to several stability and accuracy algorithms, and then the code cycles on to calculate everything for time $t + \delta t$. The output is edited in the form of graphics and files on fiche or in movies if desired.

In particular we edit plots of momentum vectors and contours of density, temperature, pressure, and the accelerating potential. Examples are displayed in subsequent figures.

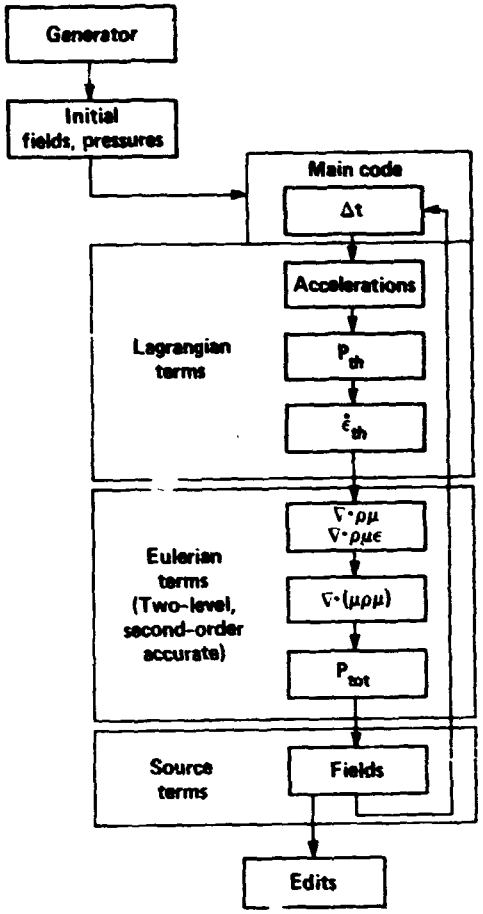

Figure 5: Flow chart for advanced Eulerian thermal hydrodynamics code of J. LeBlanc

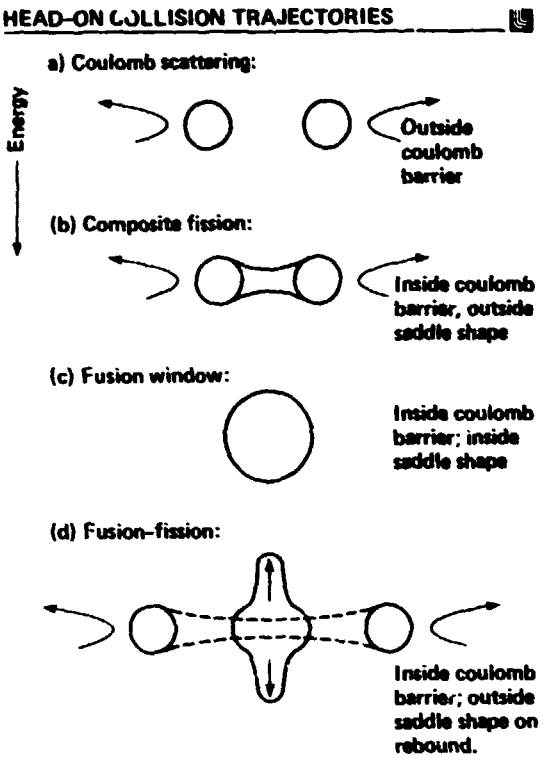

Figure 6: Possible features of symmetric heavy ion collisions as a function of projectile energy.

V. Nuclear Collisions

In this section we present a variety of collision phenomena predicted by this model, along with comparisons with other dynamic nuclear model predictions and with experimental data. At the lowest bombarding energies we do not expect our results to be accurate because we neglect predominant quantal shell effects. Low-energy collisions are subsonic and basically incompressible. When we increase the relative projectile velocity to the nuclear sound speed, around v/c = .16, the collisions become supersonic and then interesting compressible and thermal effects are predicted. Of course in a detailed thermal calculation the compressibility

$$K = 9\rho^2 \frac{\partial^2 \epsilon}{\partial \rho^2} \tag{14}$$

depends on the local state of the matter, and therefore so does the sound speed

$$C_s = \left.\frac{\partial P}{\partial \epsilon}\right|_s \tag{15}$$

If local conditions are such that C_s is smaller than in the stiff ground-state nuclear matter, then interesting compressions are possible.

In our collision calculations we are seeking detailed knowledge about such thermal compression effects. Our hope is that with detailed thermal understanding we will have more control over predicting the compression and dynamics than has heretofore been possible. We shall now review generally what happens in these collisions as the projectile energy is increased.

1. Head-On Collision Trajectories

Figure 6 illustrates head-on collisions, in the center-of-mass system, of two identical nuclei. Five general types of process are possible, in order of increasing energy. If the incoming kinetic energy is so low that the long-range Coulomb repulsion absorbs all the initial kinetic energy before the shorter-range nuclear forces can fuse the nuclei together, then the nuclei turn around and accelerate backward, as shown in trajectory (a). At slightly higher energies the attractive "proximity force" (which is like the molecular Van der Waals force) can partially fuse the nuclei. If the initial kinetic energy is used up before a stable "saddle shape" is reached, then the repulsive Coulomb forces predominate and the partially fused system separates again, as in trajectory (b).

At even higher energies it is possible, at least for the lighter nuclei, to fuse the composite system inside the saddle shape (where attractive nuclear forces just balance the repulsive Coulomb forces), at the same time absorbing most of the initial kinetic energy. This results in a stable fused compound nucleus as in (c). At medium-high energies the nuclei fuse to form a flat disk, which then rebounds out to an elongated spheroid. Here the kinetic energy remains so high that the system fissions on rebound, producing the fusion-fission process of trajectory (d). These higher-energy collisions can result in some exotic shapes. Finally, at relativistic energies the nuclei tend to splat into an expanding disk whose disintegration was discussed by the previous speaker.

The existence of a "fusion window" (c) between composite fission (b) and fusion-fission (d) depends on the size of the compound system. Theoretically a compound nucleus with no kinetic energy reserves will undergo fission if its "fissility"

$$X \sim 0.02\, Z^2/A = \text{Coulomb energy/surface energy} \qquad (16)$$

exceeds unity. For head-on collisions this occurs roughly for identical projectiles heavier than Sm. Thus we would predict that colliding Ca nuclei would have a fusion window but U nuclei would not. The fusion window was of great interest a decade ago because it made the generation of "superheavy" elements possible. Subsequent experiments implied that the fusion window was much narrower than predicted, probably because of viscous dissipation during the collision. We plan to study viscous effects, but the simulations presented here are for inviscid nuclear matter.

Figure 7 shows the results of our Coulomb scattering calculation of Ca on Ca at an initial code kinetic energy of 0.5 MeV/amu in the CMS. The maximum temperature remains relatively cool at 2 MeV and the compression (ρ/ρ_o where $\rho_o = 0.145$ amu/fm^3) remains near the normal nuclear value. Our computer runs place the fusion barrier somewhere between 0.5 and 0.6 MeV/amu, while experimentally it lies at 0.66 MeV/amu. (7)

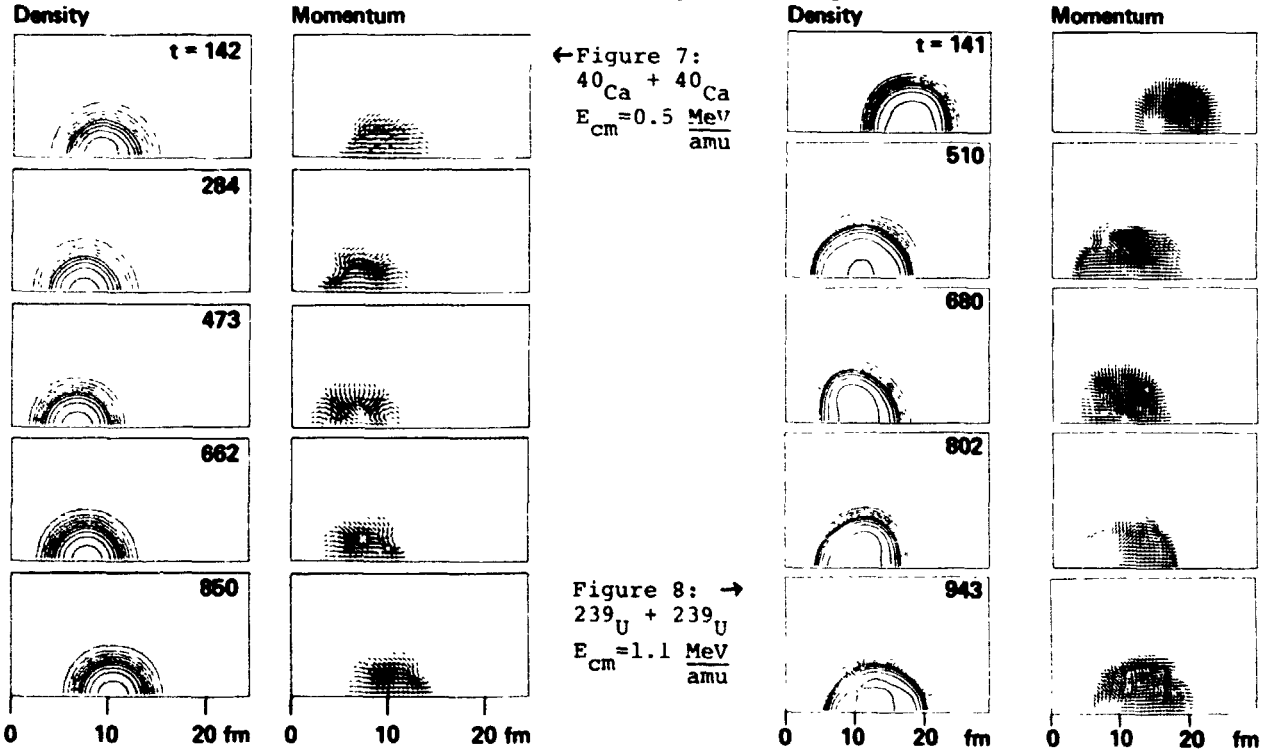

←Figure 7: $^{40}Ca + ^{40}Ca$ E_{cm}=0.5 MeV/amu

Figure 8: → $^{239}U + ^{239}U$ E_{cm}=1.1 MeV/amu

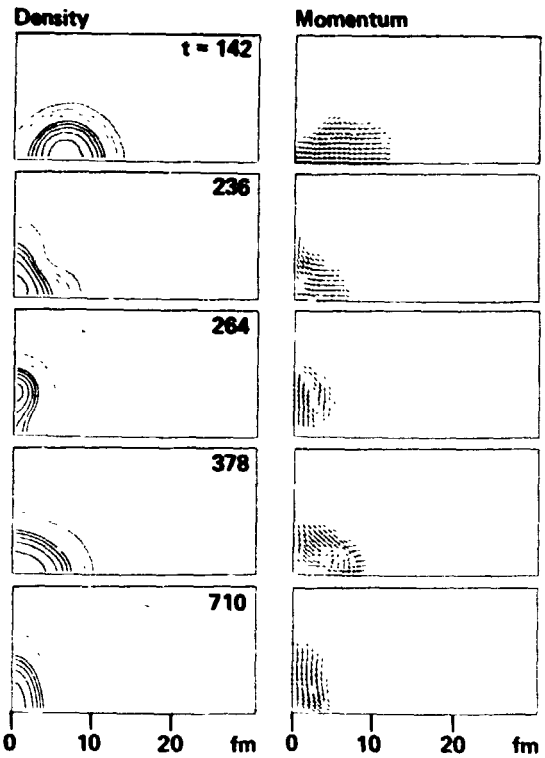

Figure 9: $^{40}Ca + {}^{40}Ca$ at E_{cm}=1.5 $\frac{MeV}{amu}$

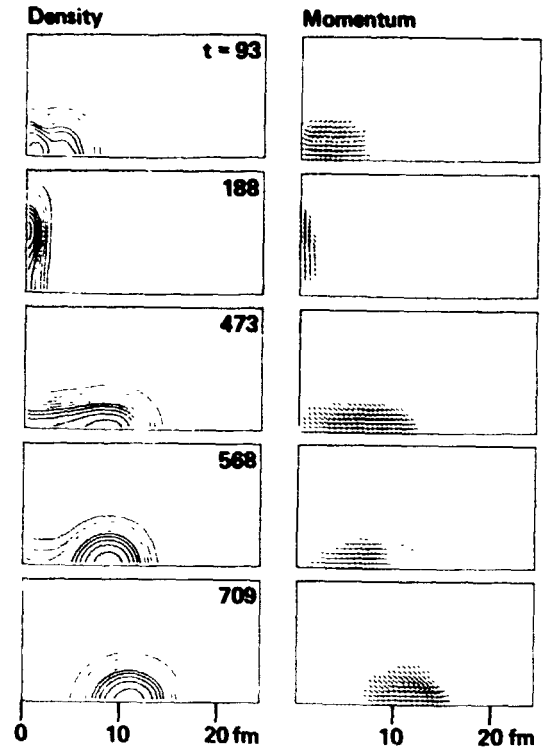

Figure 10: $^{40}Ca + {}^{40}Ca$ at E_{cm}=5 $\frac{MeV}{amu}$

That is, we currently underestimate the barrier, perhaps indicating a little too much nuclear binding. Time-dependent Hartree-Fack (TDHF) calculations, on the other hand, tend to overestimate the barrier to between 0.7 and 0.9 MeV/amu, depending on the choice of iteraction force (7).

A Coulomb scattering calculation for a ^{239}U collision is shown in Figure 8. Notice the interesting sequence of distorted shapes during closest approach.

Figure 9 shows a fusion process (Ca on Ca) at 1.5 MeV/amu. The composite system necks into a prolate spheroid and then flattens into an oblate disk, from which it rebounds into a spheroid without a neck. This fused compound nucleus then oscillates very much like a classical charged liquid drop, as shown by the later frames in Figure 9. During the initial shock of fusion the compression reached a maximum of 1.3 and the average temperature was around 5 MeV, indicating strong local heating. The temperature tends to increase quickly during the initial fusion process and then to build up slowly thereafter (see Figure 14).

Next in this sequence, Figure 10 shows a high-energy Ca on Ca collision at 5 MeV/amu which demonstrates fusion followed by fission on the rebound. Here the oblate disk gets very extended but the nuclear forces are able to pull it back so that it shoots out into an extended prolate shape which soon fissions. The maximum compression at impact was 1.4. During the expanded oblate stage the average compression was sub-nuclear at 0.7, and the average temperature cooled down to 3 MeV.

If this collision is simulated at even higher energies, then the oblate disk expands so much that it does not stop, and the composite system is presumed to disintegrate into small particles.

Thus our Ca on Ca calculations display the appropriate behavior as a function of initial kinetic energy. The dynamic fusion window for Ca on Ca appears to occur for E_{cm} between 0.6 MeV/amu and 4 MeV/amu for the case of this low-viscosity nuclear fluid. The lower limit agrees with the experimental of 0.66 MeV; the upper limit has not been measured to our knowledge. We have not yet established our upper limit precisely; it is somewhere between 3 and 5 MeV/amu.

Figure 11 displays the collision and subsequent fission of a ^{239}U system at E_{cm}=1.8 MeV/amu. The accelerating potential contours are plotted here. The collision results in a ternary fission of the composite. At lower energies a binary fission results from the collision.

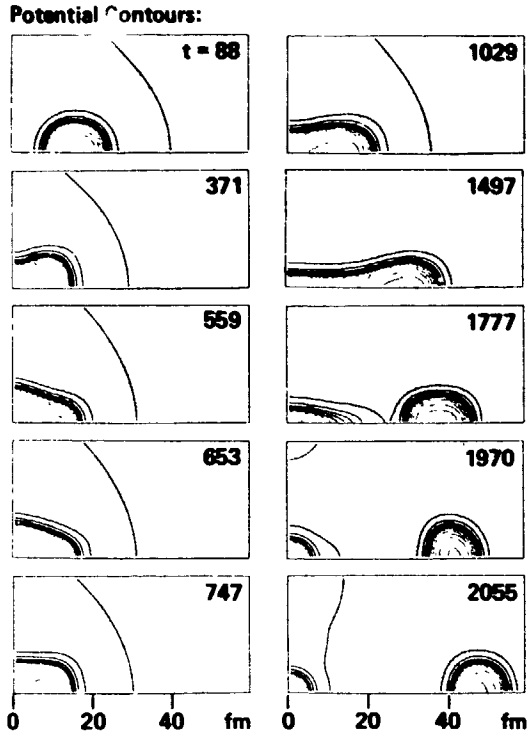

Figure 11: ^{239}U + ^{239}U at E_{cm}=1.8 $\frac{MeV}{amu}$

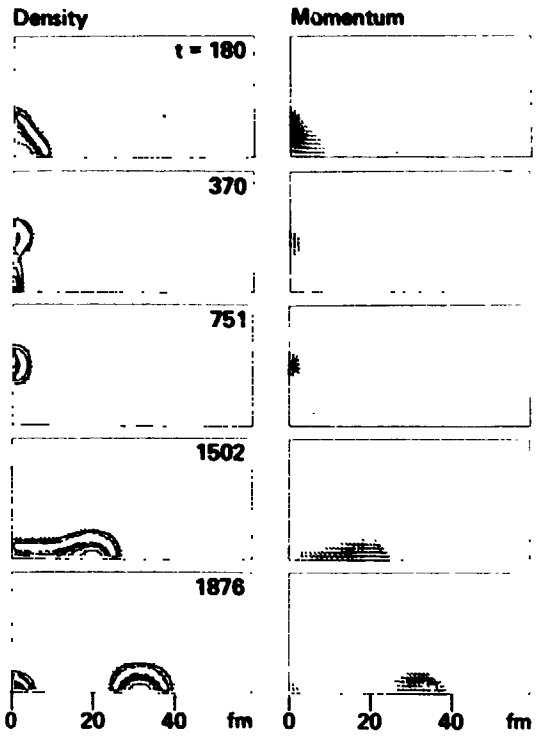

Figure 12: ^{150}Sm + ^{150}Sm at E_{cm}=5.2 $\frac{MeV}{amu}$

A final example of collision dynamics is shown in Figure 12. Here ^{150}Sm collides with itself at 5.2 MeV/amu in the center of mass. The interesting feature is the torodial shape that forms from the oblate disk. Similar toroidal shapes have been observed in TDHF calculations. We also see them in higher-energy ^{239}U collisions. The torus expands out with low compression and then collapses in on itself with high compression. The composite then fissions on the rebound.

2. Composite Nucleus Oscillations

During and after a low-energy fusion collision, the composite nucleus exhibits two kinds of oscillation. During the collision it undergoes a series of rapid energy oscillations associated with compression waves in the heated composite. After the fusion is complete the heated compound nucleus oscillates in a roughly classical liquid drop manner. These processes are exhibited in Figure 13, where we show the total kinetic energy as a function of time for the collision of two Kr nuclei at 0.5 MeV/amu in the CMS.

The period of the surface oscillations after fusion is 18×10^{-22} sec, which is close to the period predicted by the classical expression for frequency of surface oscillations of a charged liquid drop. Thus at these lower energies the thermal effects generated during the collision do not greatly affect the overall classical kinetic behavior of the compound nucleus. This predicted oscillation behavior can also be taken as evidence that our code is working reasonably at low energies.

At higher collision energies a stable compound nucleus is not formed because it fissions on rebound. The heated fission fragments, however, also undergo roughly classical oscillations as they move apart from each other.

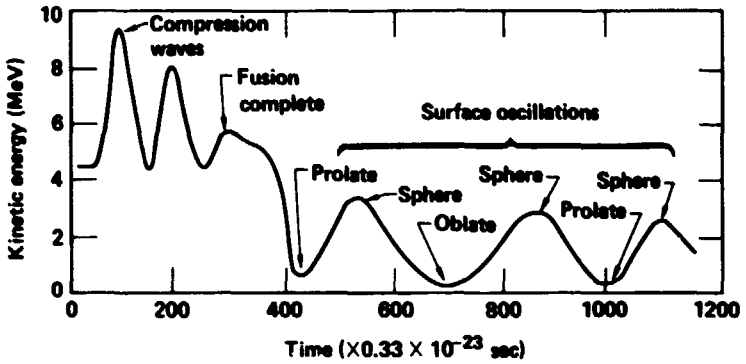

Figure 13: Kinetic energy oscillations of compound nucleus from $^{80}Kr + ^{80}Kr$ at E_{cm}=0.5 MeV/amu.

3. Compression and Heating

Above nuclear excitations of the order of 50 MeV, shell effects disappear in heavy nuclei. This corresponds to a temperature of about 6 MeV using the usual conversion for a Fermi gas: (8)

$$E^* = a T^2 \approx \left(\frac{A_1 + A_2}{8}\right) T^2 \qquad (17)$$

At such temperatures, macroscopic features like shapes and fission barriers are influenced by the excitation, and heating effects are important in medium-and high-energy nuclear physics. In collapsing stars the compressed nuclear fluid is at temperatures of 2 - 10 MeV, so thermal changes in the nuclei comprising the material could affect the bulk properties of the star. Figure 14 compares experimentally deduced fragment temperatures with the theoretical Fermi and Boltzmann limits (8).

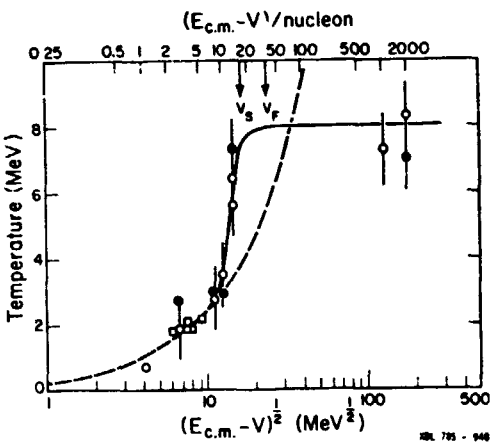

Figure 14: Nuclear Temperatures.

Compression during collisions is of great interest because of the possibility of phase changes. At twice the ground state nuclear density a pion condensation has been predicted. Figure 15 compares the maximum compressions obtained during a barely subsonic ^{40}Ca fusion-fission collision at 5 MeV/amu and a supersonic collision at 19 MeV/amu. The outstanding feature is the rapid expansion into an underdense torus for the supersonic case. This is accompanied by cooling as shown by the corresponding temperature curves in Figure 16. When the torus collapses, a compression of 1.6 results. It is possible that careful engineering of nuclear dynamics could produce compressions near 2.0. The subsonic collisions remain mostly incompressible, with some compression followed by expansion during the fusion process.

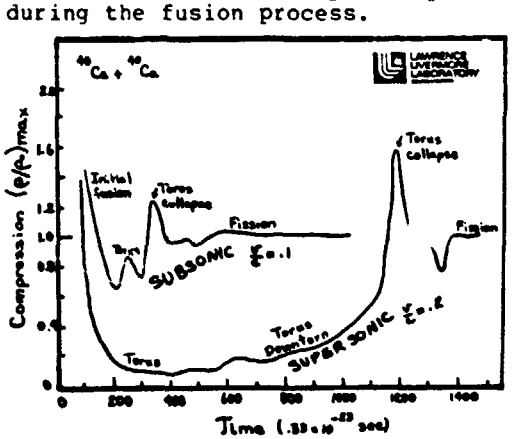

←Figure 15: Maximum compression history for ^{40}Ca on ^{40}Ca at E_{cm}=5 MeV/amu.

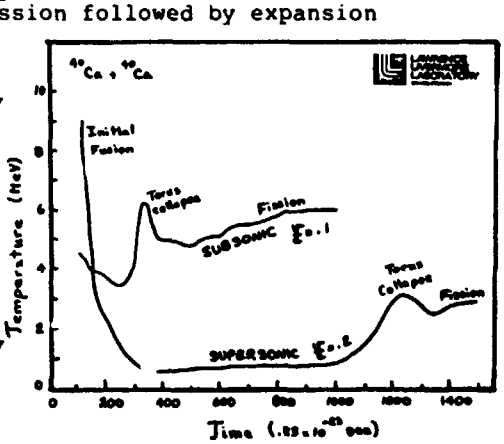

→Figure 16: Average temperature history corresponding to Figure 15.

Thermal expansion also accompanies the higher-energy collisions. As the nuclei fuse the composite heats up and expands. These thermal properties translate into a temperature-dependence for such macroscopic quantities as the surface tension, the Coulomb energy, and the volume energy, as pointed out by Sauer et. al. (9). The static thermal (T=2 MeV) Hartree-Fock calculations of the latter produced smaller changes in the density profile than we see in our heated ^{40}Ca nuclei.

At high temperatures the fission barrier is lowered due to a decrease in surface tension. We plan to study this process in more detail in the future. Conversely, nuclear material at high temperatures, as in stellar material, might be expected to exhibit different fusion windows and cross sections, both because of thermal expansion and because of softer surface density profiles. We will now discuss this interesting possibility.

4. Collisions of Heated Nuclei:

Our results for collisions of hot nuclei are very preliminary.. This type of calculation was accomplished by allowing two cold "laboratory" nuclei to execute a fusion-fission reaction, and then to let the heated fission fragments impact their mirror images by means of reflection boundary conditions on the right-hand mesh boundary. We did this in order to achieve realistic velocity, temperature, and potential profiles in the "initial" heated nucleus.

The reasons for studying collisions of hot nuclei are twofold; first, to examine nuclear collisions in the astrophysical environment; and second, to explore possible ways of creating abnormal nuclear composites using secondary collision fragments in the laboratory. The latter should really be studied using heated projectiles and cold targets, and we have begun such studies as well.

A successful fusion of the hot fission fragments from a ^{239}U ternary fusion-fission reaction is shown in Figure 17. Unfortunately our code did not edit the masses of the independent fragments, but this hot fused composite is evidently very massive, with a radius around 8.5 fm. This intriguing result should await a careful examination of this new type of calculation before it is to be believed.

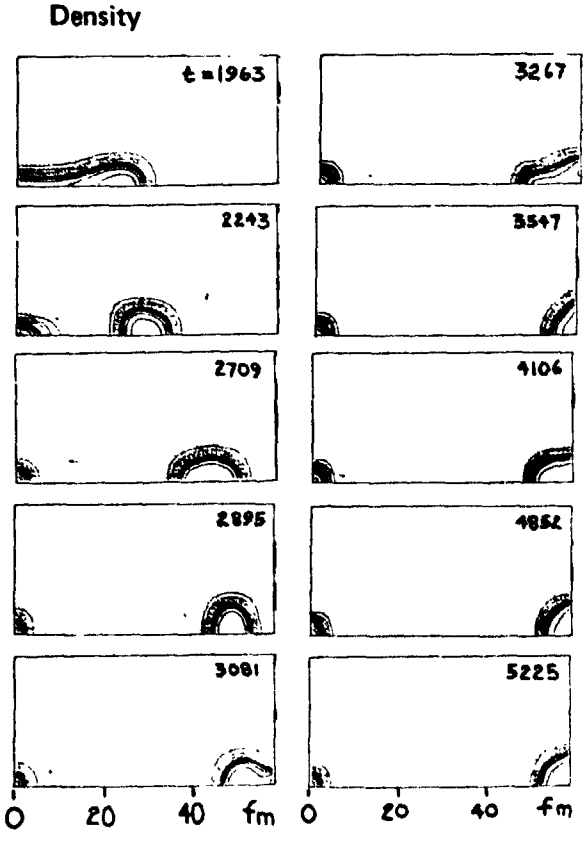

Figure 17: Collision of hot secondary fragment with its mirror image (on RHS).

The results are indeed very preliminary, but there is a suggestion here that the fusion window might be enlarged by pre-conditioning the projectile to higher temperatures or an expanded radius. (However, we have not included viscous effects yet, and the classical viscosity, which goes to $T^{1/2}$, will tend to close the fusion window.) Surface oscillations of the secondary fragment could also be used to change the fusion window if the period is engineered, for example, to present an oblate disk shape to the next target nucleus. To observe these phenomena we should concentrate on secondary reactions, tailoring the primary energy to produce the desired characteristics in the secondary.

A phenomenon which may be related has recently been reported by Friedlander et. al. (10). They observe that some secondary fragments display an anomalously short mean free path for their charge. We would like to suggest that these "anomalons" may be secondaries from central collisions that were heated and then expanded and cooled, resulting in a larger geometric cross section than would be calculated for a normal nucleus of that mass. However, for this explanation to be possible the heated nuclei would have to stay in an expanded state for very long times (10^{-11} sec). This might occur if they cannot radiate away their internal energy. We plan to investigate this possibility quantitatively.

VI. Conclusions

We have developed a computational method for treating the full thermal dynamics of nonrelativistic compressible nuclear matter. In particular we have begun a systematic study of central collisions of heavy nuclei. Preliminary results were presented for such processes as Coulomb scattering, fusion, fusion-fission, bulk oscillations, compression, heating, and collisions of heated nuclei.

Our main goal at this point was to exercise the calculation through the above variety of difficult-to-model phenomena to verify that it gives generally reasonable results. The predicted behavior in the above processes agrees qualitatively with experimental experience: e.g. low-mass projectiles fuse into a stable compound nucleus; high mass projectiles undergo a fusion-fission process; low-energy projectiles turn around under the influence of Coulomb forces; and perturbed nuclear drops oscillate in a classical manner. In producing such overall good behavior we have shown that the Wilson nuclear equation of state gives reasonable dynamical results.

We have barely begun to analyze the current predictions quantitatively. Much information is contained in these calculations. Besides reproducing some known laboratory phenomena, we have also predicted some interesting features which may or may not be real: temporary toroidal shapes are common in the higher-energy collision calculations, and the high-mass composites tend to fission in a ternary manner with a light remnant in the center of mass. These ternary processes can be checked experimentally if they persist when our calculations are made more quantitative. We also see some very preliminary evidence that pre-heated secondary nuclei can fuse more easily than cold primary nuclei. This would have important implications in both nuclear physics and astrophysics.

Our next step will be to try to systematically fine-tune the code predictions of the available experimental data to a point where the calculations are quantitatively accurate. Our immediate goal is to calculate the detailed temperature, pressure, and density gradients (including shock waves) during both cold and heated nuclear collisions. If this can be done, then the opportunities presented to us are enormous. In a long-range view, one can envision an era of nuclear fluid engineering in which one can carefully control the dynamics of nuclear collisions to produce abnormal composites, perhaps with applications totally unheard of today.

Acknowledgments

We wish to thank Virginia Taylor for typing and laying out this manuscript.

References

1. J. Wilson and R. Bowers, "Energy and Technology Review", Lawrence Livermore National Laboratory, February 1980, p. 17.
2. H. Gutbrod et. al., Phys. Rev. Lett. 37, 667 (1976)
3. A. B. Migdal, Sov. Phys. JETP 34, 1184 (1972)
4. T. H. R. Skyrme, Nuc Phys 9, 615 (1959)
5. J. D. Walecka, Annals of Physics 83, 491 (1974)
6. H. Stocker, R. Y. Cusson, J. A. Maruhn, and W. Greiner, Z. Physik A294, 125 (1980)
7. David Scott, LBL-7727, 74 (1978)
8. David Scott, LBL-7727, 117 (1978)
9. G. Saver, H. Chandra, and U. Mosel, Nuc. Phys. A264, 221 (1976)
10. E. M. Friedlander et. al., Phys. Rev. Lett. 45, 1084 (1980)